

This is the accepted manuscript made available via CHORUS. The article has been published as:

Photostrictive Two-Dimensional Materials in the Monochalcogenide Family

Raad Haleoot, Charles Paillard, Thaneshwor P. Kaloni, Mehrshad Mehboudi, Bin Xu, L. Bellaiche, and Salvador Barraza-Lopez

Phys. Rev. Lett. **118**, 227401 — Published 30 May 2017

DOI: [10.1103/PhysRevLett.118.227401](https://doi.org/10.1103/PhysRevLett.118.227401)

Photostrictive two-dimensional materials in the monochalcogenide family

Raad Haleoot,^{1,2} Charles Paillard,^{1,3} Thaneshwor P. Kaloni,¹ Mehrshad Mehboodi,¹ Bin Xu,^{1,3} L. Bellaiche,^{1,3} and Salvador Barraza-Lopez^{1,*}

¹*Department of Physics, University of Arkansas, Fayetteville, AR 72701, USA*

²*Department of Physics at the College of Education, University of Mustansiriyah, Baghdad, Iraq*

³*Institute for Nanoscience and Engineering, University of Arkansas, Fayetteville, AR 72701, USA*

Photostriction is predicted for group IV monochalcogenide monolayers, two-dimensional ferroelectrics with rectangular unit cells (the lattice vector \mathbf{a}_1 is larger than \mathbf{a}_2) and an intrinsic dipole moment parallel to \mathbf{a}_1 . Photostriction is found to be related to the structural change induced by a screened electric polarization (i.e., a converse piezoelectric effect) in photoexcited electronic states with *either p_x or p_y (in-plane) orbital symmetry* that leads to a compression of a_1 and a comparatively smaller increase of a_2 for a reduced unit cell area. The structural change documented here is ten times larger than that observed in BiFeO₃, making monochalcogenide monolayers an ultimate platform for this effect. This structural modification should be observable under experimentally feasible densities of photoexcited carriers on samples that have been grown already, having a potential usefulness for light-induced, remote mechano-opto-electronic applications.

A truly novel opto-mechanical coupling in two-dimensional (2D) ferroelectric materials awaits to be discovered. Photostriction—the creation of non-thermal strain upon illumination [1–4]—has been well-documented in three-dimensional ferroelectrics such as SbSI [5] and BiFeO₃ [6, 7]. It has been suggested to be driven by the large voltage build-up caused by a photovoltaic effect and the resulting converse piezoelectricity [8], and it may be useful for applications such as remotely-switchable memory devices [9] and light-induced actuators [10]. The earliest studied photostrictive material, SbSI, transitions from a ferroelectric to a paraelectric at a critical temperature $T_c < 300$ K. As photostrictive effects are larger in the ferroelectric phase, T_c can be increased above 300 K on SbSI ceramics which have smaller domain sizes and display a non-uniform stoichiometry nevertheless. The photostriction response time increases with sample thickness due to a reduced penetration depth, being a few seconds on bulk samples [5]. On the other hand, ferroelectric films show photostriction within a few picoseconds [11–15], and even when the photoexcited electron-hole pair is localized [16, 17].

The growing interest on the interactions of light with 2D materials [18–21] makes a study of illumination leading to non-trivial structural deformations an interesting and timely endeavor. As long as a photoexcited state induces some amount of charge redistribution—which is a quite reasonable physical assumption—any material is expected to change shape as the structure is let to relieve the stress induced by the photoexcited carriers. Here, the surprising result is the *rather large magnitude of such structural change for 2D ferroelectrics*, that originates from an inverse piezoelectric effect upon illumination.

Two-dimensional ferroelectrics in the group-IV monochalcogenide monolayer family (GeS, GeSe, SnS, SnSe, among others) [22–31] undergo a ferroelectric-to-paraelectric transition with a transition temperature that is tunable by atomic number [25]. *Ferroelectricity*

originates from the non-centrosymmetric unit cells depicted in Fig. 1(a). Due to structural symmetry, the electric dipole \mathbf{P}_0 is zero along the y - and z -directions, and finite along the x -direction, as illustrated by two red horizontal arrows in Fig. 1(a), top view. P_0 is related to the projection of the vector joining atoms 1 and 2 (3 and 4) along the x -axis, and to how delocalized the electronic charge is. The structural side view in Fig. 1(a) includes an electronic isosurface of $0.3 \text{ e}/\text{\AA}^3$, intended to display delocalization qualitatively. The horizontal separation between group-IV and chalcogen atoms, and the degree of localization of electrons yields $P_0 = 0.60, 2.77, \text{ and } 2.06 \times 10^{-10} \text{ C/m}$ for GeS, SnS, and SnSe, respectively, despite of the longer horizontal separation of ions on GeS. Lattice parameters for ground-state structures shown in Fig. 1(a) are $a_{1,0} = 4.4736 \text{ \AA}$ and $a_{2,0} = 3.6655 \text{ \AA}$ for GeS, $a_{1,0} = 4.3087 \text{ \AA}$ and $a_{2,0} = 4.0786 \text{ \AA}$ for SnS, and $a_{1,0} = 4.4038 \text{ \AA}$ and $a_{2,0} = 4.2918 \text{ \AA}$ for the SnSe monolayer.

Photostriction of SnS and SnSe is successfully predicted hereby, following the numerical approach proven to capture photostriction of BiFeO₃ [10] (*photostriction of GeS is also demonstrated as Supplementary Material (SM)*). Screening of the electric dipole due to photoexcitation will be shown to be the main driver of the *structural distortion*. This effect could be readily observed in recent experimental setups such as the one in Ref. [26].

The challenge at hand and the computational approach are described first. Then, the two direct optical transitions to be employed to demonstrate the effect are motivated, and the anisotropic change of lattice parameters (photostriction) upon photoexcitation is documented. The decrease of the dipole moment and unit cell area seen in our numerical results are explained in terms of a photoinduced inverse piezoelectric effect and electronic pressure afterwards.

The concept is straightforward: one creates the effect of a direct optical transition at the valence and conduc-

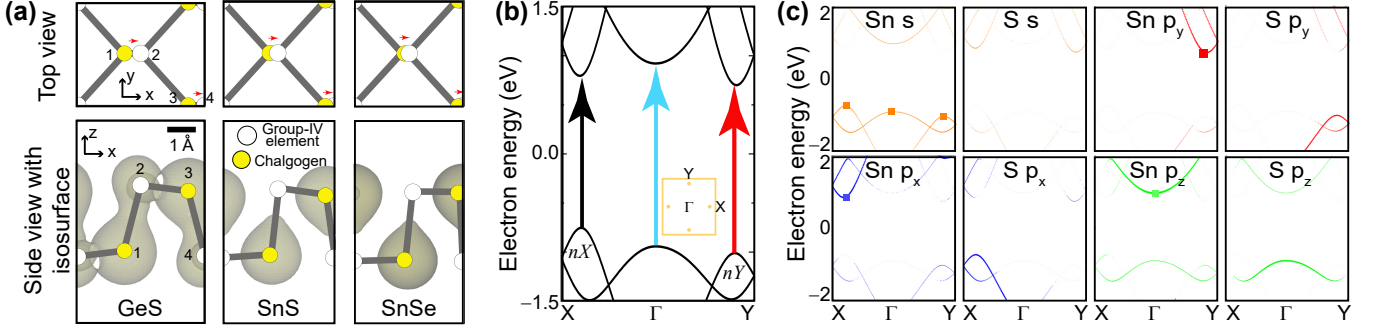


FIG. 1. (a) Unit cells for GeS, SnS, and SnSe monolayers. Red arrows on top views illustrate the direction of the electric dipole allowed by symmetry. A $0.3 \text{ e}/\text{\AA}^3$ isosurface on the side view illustrates delocalization of electronic charge. (b) Bandstructure of SnS monolayer, displaying three direct optical transitions. A first Brillouin zone inset displays the $\pm nX$ and $\pm nY$ band edges as dots. (c) Orbital-resolved electronic structure of the SnS monolayer, with probability related to the observed line thickness. Optical transitions among valence band edge states with s symmetry (orange squares) and conduction band edge states with p_x , p_y , or p_z character at the nX , nY , or Γ band edges (highlighted by squares) are allowed by symmetry.

tion band edges, allowing the structure to relax the forces created in the photoexcited state. Even though these materials are indirect band-gap semiconductors (gray arrow in Fig. 1(b)), the direct transitions shown by vertical arrows in Fig. 1(b) bring carriers onto the bottom of electron valleys. The two valleys near the corners of the first Brillouin zone are located at $0.390\mathbf{b}_1$ (nX) and $0.415\mathbf{b}_2$ (nY) for SnS (Fig. 1(b); \mathbf{b}_1 and \mathbf{b}_2 are reciprocal lattice vectors), and at similar locations for GeS and SnSe (SM).

These direct transitions are unlike indirect transitions in materials like silicon or bulk dichalcogenides, where photoexcited electrons are never excited into a local valley and quickly release energy by coupling to lattice vibrations on their way into the band minima. In the present case, excited electrons face up-hill energy bands in all directions due to the positive curvature of the local valleys, which may confine electrons sufficiently long for them to decay onto the valence band with non-negligible probability and preserving linear momentum.

In practice, capturing the effect requires approximations: specifically, the accuracy in forces needed to observe photostriction makes the Bethe-Salpeter approach [32, 33]—the technique of choice for optical excitations in materials of reduced dimensionality—prohibitively expensive, and the same could be said of a time-dependent approach to the problem [34]. Indeed, photostriction under a density of photoexcited carriers n_c changes lattice parameters $|\Delta a_i/a_{i,0}| \equiv |(a_i(n_c > 0) - a_{i,0})/a_{i,0}|$ ($i = 1, 3$) to within $10^{-5} - 10^{-4}$ in bulk samples [3], making for a prohibitively expensive optimization of the electron-hole-pair hosting structure ($a_{i,0} \equiv a_i(n_c = 0)$ here).

However, the recent discovery of ferroelectricity in monochalcogenide monolayers [25, 26] gives an opportunity to extend this well-known effect into 2D materials, and the structural deformation in photoexcited monochalcogenide monolayers will be demonstrated using the technique [10] that successfully reproduces the

experimentally observed photostriction of BiFeO₃ [35].

Görling formulated the interacting, photoexcited Hamiltonian as a model non-interacting DFT Hamiltonian [36], and the Δ -self-consistent-field (Δ SCF) method is a realization of Görling’s approach that assumes a one-to-one correspondence between the excited states of a Kohn-Sham Hamiltonian and the real system [37]. It creates a population imbalance akin to that produced from illumination, by depleting a finite number of electrons in the valence band and promoting them onto higher energy bands. Δ SCF calculations of excited states for systems with reduced dimensions abound (e.g., Refs. [38–40]), and the Δ SCF method as implemented in the *ABINIT* code [41] is employed to predict structural effects of direct optical transitions on ferroelectric monochalcogenide monolayers here. Calculations were performed on periodic structures with GBRV projected-augmented-wave [42] pseudopotentials [43] of the PBE type [44], which are known to underestimate the electronic band gap. Nevertheless, additional corrections make it prohibitive to demonstrate the effect within computational constraints.

Figure 1(c) shows the electronic structure of SnS decomposed in states with s , p_x , p_y or p_z orbital symmetry and belonging to a specific atomic species (Sn or S); projected band structures for GeS and SnSe, displaying similar trends, are provided as SM. Line thicknesses reflect the relative probability of finding a given orbital symmetry for a given band and chemical element. Optical transitions require non-zero matrix elements $\langle p_{i,c}|\mathbf{r}|s_v\rangle$ for wavefunctions with $|p_i\rangle$ symmetry in the conduction band and $|s\rangle$ symmetry in the valence band ($i = x, y, z$). According to Fig. 1(c), the group-IV element (Sn) has an orbital s -symmetry at the nX and nY valence band edges (as emphasized by orange rectangles at such band edges; this is the case for GeS and SnSe too (SM)). Similarly, a large probability is carried by Sn orbitals with p_x (p_y) symmetry at the nX (nY) conduction valley edge

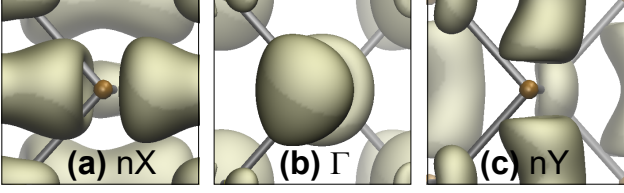


FIG. 2. SnS monolayer states at the valence band and the nX , Γ , and nY conduction local valley minima have p_x , p_z , and p_y orbital symmetries, respectively. Direct optical transitions at the nX and nY k -points perturb in-plane orbitals and will lead to the largest photostriction.

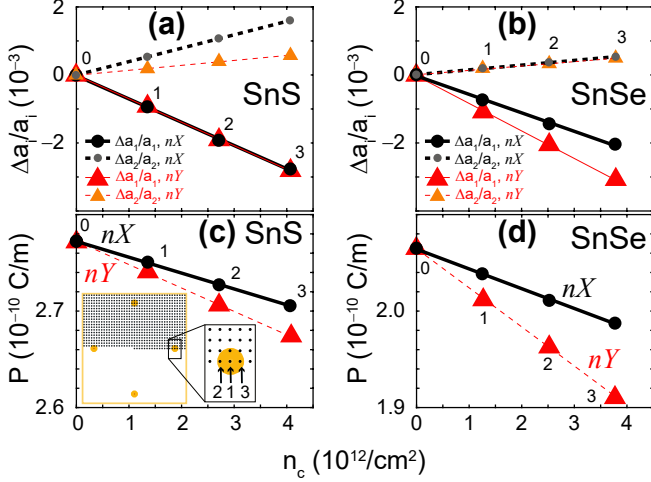


FIG. 3. Photostriction, a non-thermal change of a_1 and a_2 upon irradiation by light is demonstrated for (a) SnS and (b) SnSe monolayers. The change on a_1 and a_2 is one order of magnitude larger than that for BiFeO₃, under experimentally accessible excited carrier densities. (c)-(d) Photostriction decreases P . The inset in subplot (c) shows the k -point mesh employed (the remainder of the Brillouin zone is included by symmetry), and the zoom-in exemplifies three k -points ($n = 1, 2, 3$) photoexcited about the nX point.

(red rectangles). This way, the non-zero $\langle p_{i,c} | \mathbf{r} | s_v \rangle$ matrix element originates from a Sn *intra-atomic* direct optical transition with linearly-polarized absorption band edges [28, 45]. (Incidentally, one also notes that a direct optical transition at the Γ -point would lead to an excited state with out-of-plane (p_z) symmetry.)

Illumination by pulsed laser sources can generate photoexcited carrier density fluences as high as $10^{13} - 10^{14}/\text{cm}^2$ on MoS₂ samples [46]. It will be shown that a much smaller density is needed for the effect being presently described to be experimentally achievable, after discussing the k -point mesh employed in calculations.

Considering spin-orbit coupling (SOC), a regular 2D mesh containing n_k^2 equally-weighted k -points yields a density of $n_c = 1/(n_k^2 A_0)$ charge carriers per band per k -point per unit cell. The k -point mesh with $n_k = 41$ —shown as an inset in Fig. 3(c)—permits creating $n_c(n) =$

$2^2 n / (41^2 A_0) \simeq 1.3 n \times 10^{12} / \text{cm}^2$ excited charge carriers per band per unit cell. Here, the factor of four is due to the symmetry of the k -point mesh shown at the inset, and because carriers from two bands immediately below the bandgap are excited into two bands right above the bandgap that are slightly split due to SOC; the dependence of n_c on $n = 0, 1, 2$ or 3 allows for a gradual increment of photoexcited carriers. Recalling that photostriction of bulk samples results on $|\Delta a_i|/a_{i,0} \simeq 10^{-4} - 10^{-5}$ [3, 10, 35], a demanding relaxation limit for structural forces of 5×10^{-8} Ha/Bohr and an energy cutoff of 40 Ha were employed in our calculations.

Figure 2 displays the orbital character of the conduction band at the nX , Γ and nY k -points prior to structural optimization. The orbital character of these transitions determines the strength of the photostrictive effect.

Indeed, Figs. 3(a) and 3(b) display a decrease of a_1 ($a_1(n_c > 0) < a_{1,0}$) and an increase of a_2 ($a_2(n_c > 0) > a_{2,0}$) for both SnS and SnSe monolayers. More specifically, the ratio $\Delta a_1(n_c)/\Delta a_2(n_c)$ is equal to -0.58 for the nX transition and -0.21 at the nY transition for SnS. In SnSe, $\Delta a_1(n_c)/\Delta a_2(n_c) = -0.26$ (nX) and -0.16 (nY). (For reference, Poisson ratios are 0.36 and 0.42 for SnS and SnSe, respectively [47].) In addition, a compression of the unit cell area A versus n_c ($A < A_0$) is found (SM). Figs. 3(a-b) contain the first prediction of photostrictive effects in 2D materials; they open a completely unexplored door for studies of coupled mechano-opto-electronic effects on 2D compounds.

Furthermore, the rather large change on a_1 and a_2 in Figs. 3(a-b) ($|\Delta a_i/a_{i,0}| \sim 10^{-3}$) (under experimentally accessible photoexcited charge carrier densities $n_c \sim 10^{12}/\text{cm}^2$ [46]) is one to two orders of magnitude larger than that reported for bulk ferroelectrics and hence quite encouraging: such large values of $\Delta a_i/a_{i,0}$ place these new photostrictive 2D materials in a class of their own. A similar photostriction and decrease of P for GeS (SM) confirms the findings for SnS and SnSe, thus implying a generality of the effect on members of this material family for which $a_1 \neq a_2$.

As indicated earlier, charge rearrangement is bound to occur upon photoexcitation and regardless of the numerical method employed (i.e., that in Refs. [32, 33], Ref. [34], or the present one [36, 37, 41], which permits a comparatively small time-consuming tracking of the structural distortion). Local exciton wavefunctions on GeS and GeSe shown in Ref. [45] will also necessarily perturb the initial electric dipole, and will lead to a structural distortion akin to the one shown here. Although numerical estimates will depend on method, the modification of the lattice structure with light is to be expected.

The effect of orbital symmetries on the magnitude of photostriction becomes manifest when testing a transition at the Γ -point for states that are deeper within the conduction and valence bands. In that case, photostriction turns negligible (SM): in-plane orbitals are naturally

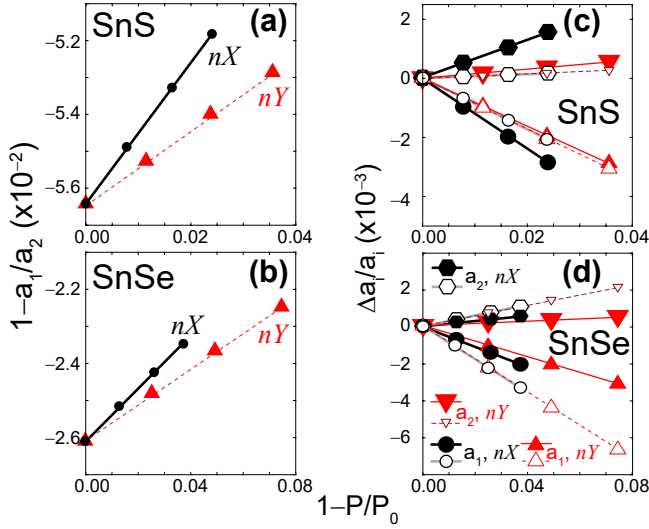


FIG. 4. (a-b) The decrease of P is linearly dependent on the ratio a_1/a_2 . (c-d) The decrease of lattice parameters with P arises from an inverse piezoelectric effect, as calculated from Eqn. 1 and shown in open symbols.

better in screening the electric dipole than out-of-plane orbitals that extend into the vacuum. On the same vein, the effect turns stronger than in the bulk because the structural change driven by screening in-plane orbitals is never counteracted from a (sturdier) 3D structure.

The reduction of P (obtained from Born effective charges) seen in Figs. 3(c-d) is related to the anisotropic change in lattice constants seen in Fig. 4(a) and 4(b) for SnS and SnSe, respectively. SnS and SnSe monolayers host an in-plane P parallel to the \mathbf{a}_1 lattice vector that becomes reduced as the ratio a_1/a_2 approaches unity [28]: this is why the polarization $P_0 \equiv P(n_c = 0) = 2.77 \times 10^{-10}$ C/m for SnS ($a_{1,0}/a_{2,0}=1.056$) is larger than that for SnSe ($P_0 = 2.06 \times 10^{-10}$ C/m, and $a_{1,0}/a_{2,0}=1.026$) already and, within a given material, the reason for the thermally-induced ferroelectric-to-paraelectric transition for a sudden change of the structural order parameter $a_{1,0}(T)/a_{2,0}(T)$ towards unity without illumination, where $P_0(T_c)$ goes all the way to zero [28, 30] at the transition temperature T_c . Photostriction is a new (optical) handle to reduce a_1 and increases a_2 , regardless of valley edges being excited (nX , nY , Γ , or nX -to- nY (indirect)).

We showed the tunability of a_1 and a_2 with chemistry [25] and temperature [28]. Presently, the remarkable tunability under illumination is to be understood from an inverse piezoelectric effect [10] as follows. In 2D, the dielectric susceptibility χ_i^{2D} and the dielectric tensor ϵ_i (both diagonal) are related as $\chi_i^{2D} = \frac{(\epsilon_i-1)}{4\pi}L$ [48–50], where L is the vertical separation between (periodic) layers. This way, using the numerical change in polarization $P - P_0$ (which only occurs along the x -axis) and considering the $mm2$ point-symmetry of these compounds,

TABLE I. In-plane stress (in GPa) prior to structural relaxation arising from photoexcitation at the nX and nY points for $n_c(1)$. $\Delta a_i/a_{i,0}$ ($i = 1, 2$) below must be scaled by 10^{-4} .

SnS				SnSe			
nX	nX	nY	nY	nX	nX	nY	nY
σ_{xx}	σ_{yy}	σ_{xx}	σ_{yy}	σ_{xx}	σ_{yy}	σ_{xx}	σ_{yy}
0.029	0.023	0.023	0.029	0.027	0.024	0.024	0.026
Δa_1	Δa_2	Δa_1	Δa_2	Δa_1	Δa_2	Δa_1	Δa_2
$a_{1,0}$	$a_{2,0}$	$a_{1,0}$	$a_{2,0}$	$a_{1,0}$	$a_{2,0}$	$a_{1,0}$	$a_{2,0}$
-8.3	0.5	-4.6	-1.9	-7.9	-0.3	-6.1	-1.3

lattice parameters a_i ($i = 1, 2$) must evolve as [48, 51]:

$$\frac{\Delta a_i}{a_{i,0}} = \frac{d_{i1}}{8\pi\epsilon_0\chi_1^{2D}}(P - P_0), \quad (1)$$

as represented by the open symbols in Figs. 4(c-d). χ_1^{2D} is taken as is from Ref. [48] –and expressed in Å– and relaxed-ion values for d_{i1} were taken from Ref. [47]; ϵ_0 is the permittivity of vacuum [52]. These predicted trends are of the same order of magnitude to the values of a_1 and a_2 determined upon a full optimization of the photoexcited structure, and they imply that photostriction is primarily produced by an inverse piezoelectric effect due to a dipole screening by the photoexcited charge carriers.

Note that the slope in Eqn. 1 is independent of the valley being photoexcited (nX or nY), making the predicted values for $\Delta a_i/a_{i,0}$ lie upon the same straight line. The actual polarization is slightly different when exciting the nX or the nY valley.

Electronic/hole pressure may also produce slight differences in slope when exciting different valleys. Elongation of in-plane lattice vectors leads to positive stress. But when let to relax, the material *contracts* back to its original structure. In general, any structure with positive stress will contract in response. Therefore, in a first approximation, the lattice also displays an elastic *response* (having a *negative* sign) given by:

$$\frac{\Delta a_i}{a_{i,0}} = C_{ij}^{-1}(-\sigma_j). \quad (2)$$

Using the elastic coefficients from Ref. [48], and the in-plane stress recorded in Table I for $n_c(1)$ from the initial photoexcited structure *prior to any structural relaxation*, we obtain changes of $\Delta a_i/a_{i,0}$ from Eqn. (2) that are an order of magnitude smaller than those seen in Fig. 4(c-d). This way, the numerical results from the structural optimization must be dominated by the inverse piezoelectric effect, thus showing the relevance of ferroelectricity for this effect to occur in 2D materials.

The trends in Figs. 3-4 are similar to those for BiFeO₃, which implies similar mechanisms at play. Experimental realization of ferroelectric 2D monochalcogenide monolayers [26] (with no substantial depolarization fields due to size effects) enhances the present relevance of this work, and brings optimism in that the unique effects here described will soon be experimentally verified.

In conclusion, photostriction of group IV monochalcogenides has been predicted. Photostriction decreases the larger lattice vector a_1 and increases of the smaller one a_2 . It mainly arises from an inverse piezoelectric effect that reduces the dipole moment in the unit cell and contracts the lattice vector that is parallel to the electric dipole. These results continue to highlight unique properties of two-dimensional ferroelectrics and their potential usefulness for mechano-opto-electronic applications.

We thank H. Churchill, B. Hamad and S. Sharifzadeh for discussions. R. Haleoot was funded by The Higher Committee For Education Development of Iraq. T. K., M. M. and S. B.-L. were funded by the US DOE (Grant DE-SC0016139). C.P. thanks the support from DARPA Grant No. HR0011-15-2-0038 (MATRIX program). B.X. and L.B. acknowledge the US AFOSR Grant No. FA9550-16-1-0065. Calculations were performed at SDSC's *Comet* (XSEDE TG-PHY090002).

* sbarraza@uark.edu

- [1] I. Tatsuzaki, K. Itoh, S. Ueda, and Y. Shindo, *Phys. Rev. Lett.* **17**, 198 (1966).
- [2] V. M. Fridkin et al., *Appl. Phys. Lett.* **10**, 354 (1967).
- [3] B. Kundys, *Appl. Phys. Rev.* **2**, 011301 (2015).
- [4] C. Paillard, X. Bai, I. C. Infante, M. Guennou, G. Geneste, M. Alexe, J. Kreisel, and B. Dkhil, *Adv. Mater.* **28**, 5153 (2016).
- [5] A. Dogan, P. Poosanaas, I. R. Abothu, S. Komarneni, and K. Uchino, *J. Ceramic Soc. Japan* **109**, 493 (2001).
- [6] B. Kundys, M. Viret, D. Colson, and D. Kundys, *Nat. Mater.* **9**, 803 (2010).
- [7] B. Kundys, M. Viret, C. Meny, V. Da Costa, D. Colson, and B. Doudin, *Phys. Rev. B* **85**, 092301 (2012).
- [8] V. Fridkin, *Photoferroelectrics*, 1st ed., Springer Series in Solid-State Sciences, Vol. 9 (Springer, Berlin, 1979).
- [9] V. Iurchuk et al., *Phys. Rev. Lett.* **117**, 107403 (2016).
- [10] C. Paillard, B. Xu, B. Dkhil, G. Geneste, and L. Bellaiche, *Phys. Rev. Lett.* **116**, 247401 (2016).
- [11] Z. Jin, Y. Xu, Z. Zhang, X. Lin, G. Ma, Z. Cheng, and X. Wang, *Appl. Phys. Lett.* **101**, 242902 (2012).
- [12] D. Daranciang et al., *Phys. Rev. Lett.* **108**, 087601 (2012).
- [13] H. Wen et al., *Phys. Rev. Lett.* **110**, 037601 (2013).
- [14] P. Ruello, T. Pezeril, S. Avanesyan, G. Vaudel, V. Gusev, I. C. Infante, and B. Dkhil, *Appl. Phys. Lett.* **100**, 212906 (2012).
- [15] M. Lejman, G. Vaudel, I. Infante, P. Gemeiner, V. Gusev, B. Dkhil, and P. Ruello, *Nat. Commun.* **5**, 4301 (2014).
- [16] D. Schick et al., *Phys. Rev. Lett.* **112**, 097602 (2014).
- [17] H. Wen, M. Sassi, Z. Luo, C. Adamo, D. G. Schlom, K. M. Rosso, and X. Zhang, *Sci. Rep.* **5**, 15098 (2015).
- [18] A. Castellanos-Gomez, *Nat. Photonics* **10**, 202 (2016).
- [19] W. Xiaomu et al., *Nat. Nanotech.* **10**, 517 (2015).
- [20] D. N. Basov, M. M. Fogler, and F. J. García de Abajo, *Science* **354** (2016), 10.1126/science.aag1992.
- [21] D. N. Basov and M. M. Fogler, *Nat. Nanotech.*, advance online publication (2016).
- [22] G. A. Tritsarlis, B. D. Malone, and E. Kaxiras, *J. Appl. Phys.* **113**, 233507 (2013).
- [23] A. K. Singh and R. G. Hennig, *Appl. Phys. Lett.* **105**, 042103 (2014).
- [24] Z. Zhu, J. Guan, D. Liu, and D. Tománek, *ACS Nano* **9**, 8284 (2015).
- [25] M. Mehboudi et al., *Nano Lett.* **16**, 1704 (2016).
- [26] K. Chang et al., *Science* **353**, 274 (2016).
- [27] M. Wu and X. C. Zeng, *Nano Lett.* **16**, 3236 (2016).
- [28] M. Mehboudi, B. M. Fregoso, Y. Yang, W. Zhu, A. van der Zande, J. Ferrer, L. Bellaiche, P. Kumar, and S. Barraza-Lopez, *Phys. Rev. Lett.* **117**, 246802 (2016).
- [29] P. Z. Hanakata, A. Carvalho, D. K. Campbell, and H. S. Park, *Phys. Rev. B* **94**, 035304 (2016).
- [30] R. Fei, W. Kang, and L. Yang, *Phys. Rev. Lett.* **117**, 097601 (2016).
- [31] H. Wang and X. Qian, *arXiv:1606.04522* (2016).
- [32] L. Hedin, *Phys. Rev.* **139**, A796 (1965).
- [33] M. S. Hybertsen and S. G. Louie, *Phys. Rev. B* **34**, 5390 (1986).
- [34] C. A. Ullrich, *Time-Dependent Density-Functional Theory, Concepts and Applications*, 1st ed. (Oxford U. Press, N. Y., 2012).
- [35] B. Kundys, M. Viret, D. Colson, and D. O. Kundys, *Nat. Mater.* **9**, 803 (2010).
- [36] A. Görling, *Phys. Rev. A* **59**, 3359 (1999).
- [37] R. M. Martin, *Electronic Structure: Basic Theory and Practical Methods*, 1st ed. (Cambridge U. Press, Cambridge, UK, 2004).
- [38] J. Gavnholdt, T. Olsen, M. Englund, and J. Schiøtz, *Phys. Rev. B* **78**, 075441 (2008).
- [39] Y. Kitaoka, K. Nakamura, T. Akiyama, T. Ito, M. Weinert, and A. J. Freeman, *Phys. Rev. B* **87**, 205113 (2013).
- [40] K. Nawa, Y. Kitaoka, K. Nakamura, H. Imamura, T. Akiyama, T. Ito, and M. Weinert, *Phys. Rev. B* **94**, 035136 (2016).
- [41] X. Gonze et al., *Comp. Phys. Comm.* **180**, 2582 (2009).
- [42] P. E. Blöchl, *Phys. Rev. B* **50**, 17953 (1994).
- [43] K. F. Garrity, J. W. Bennett, K. M. Rabe, and D. Vanderbilt, *Comp. Mat. Sci.* **81**, 446 (2014).
- [44] J. P. Perdew, K. Burke, and M. Ernzerhof, *Phys. Rev. Lett.* **77**, 3865 (1996).
- [45] L. C. Gomes, P. E. Trevisanutto, A. Carvalho, A. S. Rodin, and A. H. Castro Neto, *Phys. Rev. B* **94**, 155428 (2016).
- [46] C. H. Lui, A. J. Frenzel, D. V. Pilon, Y.-H. Lee, X. Ling, G. M. Akselrod, J. Kong, and N. Gedik, *Phys. Rev. Lett.* **113**, 166801 (2014).
- [47] R. Fei, W. Li, J. Li, and L. Yang, *Appl. Phys. Lett.* **107**, 173104 (2015).
- [48] L. C. Gomes, A. Carvalho, and A. H. Castro Neto, *Phys. Rev. B* **92**, 214103 (2015).
- [49] P. Cudazzo, I. V. Tokatly, and A. Rubio, *Phys. Rev. B* **84**, 085406 (2011).
- [50] T. C. Berkelbach, M. S. Hybertsen, and D. R. Reichman, *Phys. Rev. B* **88**, 045318 (2013).
- [51] J. Nye, *Physical properties of crystals* (Oxford U. Press, UK, 1985).
- [52] An additional factor of two multiplying χ arises from the length scale chosen for the vertical direction: a_3 in Ref. [47], and $a_3/2$ in Ref. [48].